Newcastle University

Newcastle University ePrints

Escobedo-Cousin E, Vassilevski K, Hopf T, Wright N, O'Neill A, Horsfall A, Goss J, Cumpson PJ. Local solid phase growth of few-layer graphene on silicon carbide from nickel silicide supersaturated with carbon. *Journal of Applied Physics* 2013, 113(11), 114309.

Copyright:

Copyright 2013 American Institute of Physics. This article may be downloaded for personal use only. Any other use requires prior permission of the author and the American Institute of Physics.

The following article appeared in the Journal of Applied Physics 113, 114309 (2013) and may be found at:

http://dx.doi.org/10.1063/1.4795501

Always use the definitive version when citing.

Further information on publisher website: http://jap.aip.org

Date deposited: 1st July 2013

Version of file: Author final

This work is licensed under a Creative Commons Attribution-NonCommercial 3.0 Unported License

ePrints – Newcastle University ePrints
http://eprint.ncl.ac.uk

Local solid phase epitaxy of few-layer graphene on silicon carbide from nickel silicide supersaturated with carbon

Enrique Escobedo-Cousin*, Konstantin Vassilevski, Toby Hopf, Nick Wright, Anthony O'Neill, Alton Horsfall and Jonathan Goss

School of Electrical and Electronic Engineering, Newcastle University, Newcastle upon Tyne, NE1 7RU, United Kingdom

Peter Cumpson

School of Mechanical and Systems Engineering, Newcastle University, Newcastle upon Tyne, NE1 7RU, United Kingdom

* corresponding author: enrique.escobedo-cousin@ncl.ac.uk

Keywords: graphene, few-layer graphene, nickel silicide, silicon carbide, carbon, Raman scattering, solid phase epitaxy, X-ray photoelectron spectroscopy, Hall effect mobility.

ABSTRACT

Patterned few-layer graphene (FLG) films were grown by local solid phase epitaxy from nickel silicide supersaturated with carbon, following a fabrication scheme which allows the formation of self-aligned ohmic contacts on FLG and is compatible with conventional SiC device processing methods. The process was realised by the deposition and patterning of thin Ni films on semi-insulating 6H-SiC wafers followed by annealing and the selective removal of the resulting nickel silicide by wet chemistry. Raman spectroscopy and X-ray photoelectron spectroscopy (XPS) were used to confirm both the formation and subsequent removal of nickel silicide. The impact of process parameters such as the thickness of the initial Ni layer, annealing temperature, and cooling rates on the FLG films was assessed by Raman spectroscopy, XPS and atomic force microscopy (AFM). The thickness of the final FLG film estimated from the Raman spectra varied from 1 to 4 monolayers for initial Ni layers between 3 and 20 nm thick. Self-aligned contacts were formed on these patterned films by contact photolithography and wet etching of nickel silicide, which enabled the fabrication of test structures to measure the carrier concentration and mobility in the FLG films. A simple model of diffusion-driven solid phase chemical reaction was used to explain formation of the FLG film at the interface between nickel silicide and silicon carbide.

I. INTRODUCTION

Graphene, a single atomic layer of hexagonally arranged carbon atoms, is considered a promising candidate for numerous applications due to its unique electrical and mechanical properties [1]. Potential applications of graphene include high-speed field-effect transistors, chemical sensors and transparent electrodes [2-4]. Single layer graphene can be produced by the mechanical exfoliation of highly oriented pyrolytic graphite [2]. The chemical exfoliation of various other types of graphite has also been used to produce high quality graphene [5]. However, exfoliation methods result in irregular-shaped flakes of several microns, which are suitable for fabrication of individual devices but are not compatible with standard semiconductor device processing. Larger graphene areas can be obtained by chemical vapor deposition from carbon-containing gases on substrates made of transition metals [6], but it is difficult to control the film orientation, resulting in high cross-wafer variability of the graphene electrical properties. In addition, the graphene films formed by this method must be transferred from the metal surface onto a suitable substrate for further electronic device applications. Graphene can also be formed on semi-insulating substrates of standard size by thermal decomposition of silicon carbide (SiC) [7, 8]. This method is based on the sublimation of silicon atoms from the SiC surface and yields large area epitaxial graphene (EG) suitable for further use in electronic devices, however, temperatures exceeding 1500 °C are required to form high quality EG [9]. None of these graphene fabrication techniques is without its drawbacks, thus, new methods of graphene formation more suitable for specific applications must still be sought. One of such methods is the solid phase epitaxy (SPE) of few-layer graphene (FLG) films on silicon carbide from nickel silicide.

The interaction between a SiC substrate and deposited Ni films is one of the most thoroughly studied solid phase chemical reactions. This interaction leads to the formation of nickel silicide which is used as ohmic [10] or Schottky [11, 12] contacts in silicon carbide devices. Furthermore, nickel itself is used as a high selectivity mask for reactive ion etching of silicon carbide as well as a mask for ion implantation [12, 13]. These broad applications of nickel and nickel silicide films in SiC processing make the fabrication of FLG films from nickel silicide very attractive in terms of process compatibility. The reaction between Ni and SiC occurs at relatively low temperatures (between 600 and 1200 °C) where Si sublimation does not take place. The predominant silicide phase formed is Ni_2Si, as a result of SiC dissociation and the chemical reactions between Ni and Si, although other phases may also be present at annealing temperatures under 950 ºC [10]. Another product of this solid phase reaction is carbon which does not react with nickel and has very low diffusivity and solubility in nickel silicide [14] and nickel [15]. Following this reaction, carbon has been observed released as

precipitates in the Ni_2Si body [16,17] at the SiC/Ni_2Si interface [10], or on the top surface of the Ni_2Si contacts [18].

In 2009, Juang *et al.* [19] demonstrated FLG film formation on the surface of Ni films deposited and annealed on silicon carbide substrates. They deposited a relatively thick Ni film (200 nm) and annealed it at 750 ºC. It was proposed that carbon atoms diffused through the unreacted Ni and then segregated on its surface to form a graphene film. For further characterization the Ni underlayer was etched using an HNO_3 solution and graphene flakes were dredged up by a lacy carbon film supported by a copper grid. It has also been demonstrated that graphene can be produced by this method from initial Ni films with thicknesses of around 10 nm [20], and that ordered graphitic films can be obtained at annealing temperatures from 800 ºC [21]. Further insight into the formation of FLG films by this method was provided by studying the impact of the annealing time and temperature as well as heating ramp rate on the final graphene quality [22, 23]. It was found that the optimal annealing conditions were in the region around 800-1080 ºC. The transfer of these FLG films onto insulating substrates was demonstrated [19], but to date no results of electrical characterization of these films have been published.

In 2010, Vassilevski *et al.* [24] demonstrated that the FLG films can appear at the Ni_2Si/SiC interface instead of on the surface of unreacted nickel. Their approach was based on experimental findings of Hannel *et al.* [25] that the excess carbon forms graphitic precipitates with base planes parallel to the SiC surface in nanoscale nickel silicide films. To prove the formation of FLG films at the interface, nickel layers with thicknesses ranging from 5 to 200 nm were deposited on SiC substrates, patterned by a lift-off procedure and annealed. Then Ni_2Si was removed selectively by wet etching to form patterned FLG structures which were characterised by Raman spectroscopy and atomic force microscopy (AFM). Growth of FLG films on semi-insulating SiC wafers by this method was also demonstrated [26]. Fabricated transmission line model (TLM) structures with self-aligned contacts were used to measure the FLG sheet resistance and prove the film continuity. This method is compatible with standard device processing techniques and may enable the integration of graphene directly into silicon carbide electronic devices.

The main objective of this work was to grow FLG films by local SPE and prove their two-dimensional nature by various spectroscopic methods and direct electrical characterization. This paper presents results from patterned FLG films grown by local SPE on semi-insulating 6H-SiC substrates from nickel silicide supersaturated with carbon. FLG films were grown at the interface of nickel silicide and silicon carbide both on silicon- and carbon-terminated faces of SiC substrates. The samples were annealed at different temperatures and it was shown by Raman spectroscopy and X-ray photoelectron spectroscopy (XPS) that the process temperature and cooling rate significantly

affect the final quality of FLG films. TLM and Hall measurements on test structures with self-aligned ohmic contacts were used to measure contact resistivity, conductivity type, charge carrier density and Hall mobility in the FLG films. A simple qualitative model of diffusion-driven solid phase chemical reaction was proposed to explain the formation of FLG films at the surface of unreacted nickel or at the SiC/Ni_2Si interface, depending on growth process parameters.

II. EXPERIMENTAL DETAILS

Commercial 6H-SiC semi-insulating wafers with on-axis orientation [27] were used in this study. The FLG films were grown on the Si- and C-terminated faces of the substrate following the procedure depicted in Figure 1. Before processing, the C-terminated faces of the wafers were polished at NOVASiC [28] to a roughness R_{rms} < 0.5 nm. The Si-face of used wafers was epi-ready as supplied by the manufacturer. The samples were cleaned by degreasing with organic solvents followed by RCA cleaning procedure and oxidation in dry oxygen at 1100 °C for 6 h. The initial SiC substrate is shown in Figure 1a. After oxide removal in buffered oxide etch (BOE), nickel layers with varying thicknesses (3 to 20 nm) were deposited by e-beam evaporation at a base pressure of 1×10^{-6} Torr. The minimum thickness of Ni required to produce a FLG film can be estimated using the atomic densities of nickel, graphene, and silicon carbide. It should also be taken into account that two atoms of nickel form Ni_2Si and release one carbon atom. Assuming that the Ni_2Si and FLG films formed after annealing are continuous and do not form islands or holes, this estimation gives a minimum Ni thickness of 0.84 nm for the formation of a graphene monolayer. As a result, the FLG films formed from initially 3 nm thick Ni layers are expected to contain no more than 3 graphene monolayers. The deposited metal films were patterned using a lift-off procedure (Figure 1b). To form FLG films, the samples were annealed in a Jipelec JetFirst 200C rapid thermal processing system under high vacuum (< 10^{-4} mbar) at temperatures ranging from 700 ºC to 1080 °C (Figure 1c). Preliminary experiments with 200 nm thick Ni layers annealed on SiC were carried out in order to determine the reaction rate (~ 0.3 nm/s of Ni at 1080 °C) and minimum required annealing time to ensure that all the Ni in the thin layers (3 to 20 nm) is converted to Ni_2Si. All samples were annealed for 200 s with temperature front ramp rate of 30 °C/s. The Ni_2Si films were stripped by etching for 2 min at room temperature in Freckle etch, H_3PO_4: CH_3COOH: HNO_3: HBF_4: H_2O (70:10:5:5:10) which was found to be a selective etchant for nickel silicide [29]. When required, the removal of Ni_2Si was carried out selectively in order to form self-aligned contact pads (Figure 1d). Ti/Ag (3 nm/50 nm) contact reinforcements were deposited on top of the Ni_2Si pads by e-beam evaporation and patterned by a lift-off procedure for further electrical measurements.

The FLG films were characterized by XPS, Raman spectroscopy, AFM, TLM and Hall measurements. XPS spectra were collected using a Thermo K-alpha spectrometer using monochromatic Al Kα radiation with a source energy of 1486.68 eV and a photoemission angle $\theta = 0°$. The samples were not subjected to any treatment prior to the measurements. A Shirley-type background was subtracted and a Gaussian-Lorentzian function was used to fit the spectra. Micro-Raman spectra were collected using a LabRAM HP Raman microscope fitted with an argon ion laser. The spectra were taken at room temperature in the confocal backscattering configuration using an excitation wavelength of 514.5 nm and a 100× objective with 0.9 numerical aperture, resulting in a spot size diameter of around 700 nm. The maximum laser power delivered at the sample surface was 10 mW. The spectra for FLG films were obtained by subtracting the reference spectrum corresponding to the 6H-SiC substrate. AFM scans were taken in non-contact mode using an XE-150 AFM from Park Systems. TLM and Hall measurements were performed on-wafer at room temperature. The Hall measurements were performed in the van der Pauw geometry to extract sheet resistivity, mobility, carrier type and density, using a Hall and van der Pauw measurement system from MMR Technologies. The TLM measurements were carried out in a Cascade microtech probe station using a Kethley 4200 parameter analyser.

III. EXPERIMENTAL RESULTS AND DISCUSSION

A. Residual contamination and chemical state of FLG films grown by SPE on SiC

First of all, the formation and the removal of Ni_2Si was confirmed using Raman spectroscopy. Figure 2a compares the Raman spectra of a 20 nm thick Ni film as-deposited (dashed line) with the same film after annealing at 1080 ºC (solid line). The spectrum corresponding to the annealed film exhibits increased intensity around the 100 cm^{-1} and 140 cm^{-1} bands compared with the as-deposited Ni film, corresponding to the characteristic peaks for Ni_2Si [30], which confirms the formation of Ni_2Si. The spectrum for the FLG film following the Ni_2Si wet etching is also shown by the solid line with circles in Figure 2a. After wet etching, the FLG films exhibited low intensity in the 100 cm^{-1} and 140 cm^{-1} bands, confirming the complete removal of Ni_2Si. Removal of nickel siliside was also confirmed by XPS. Figure 2b shows narrow Ni 2*p* scans measured on the FLG before and after the wet etching of Ni_2Si. No spectra normalization was carried out. The spectrum of Ni_2Si exhibits clearly defined peaks at 870 eV and 853 eV, corresponding to the Ni $2p^{1/2}$ and Ni $2p^{3/2}$ transitions in Ni_2Si, respectively [31]. Both peaks disappear after etching, indicating that the Ni_2Si layer was removed completely, in good agreement with the Raman measurements.

XPS was also used to confirm the graphitic composition of the FLG layers following the Ni_2Si removal. Figure 3a displays the survey scan of a FLG film grown by SPE on the C-face of the SiC substrate from an initial Ni layer thickness of 7 nm, showing the main species present at the sample surface, which are carbon and oxygen. The most prominent line, located at a binding energy of 284 eV, corresponds to the graphitic sp^2 component in the C1s envelope. Figure 3b shows narrow C1*s* scans taken from the FLG films grown on the Si- and C-face of the SiC substrate by SPE. The only clear difference between the XPS spectra of FLG films grown on the Si- and C-face of the SiC was a shift in the binding energy of the sp^2 peak. It was observed that the sp^2 peak binding energy was around 0.5 eV higher for the FLG films grown on the C-face than on the Si-face. This shift can be related to substrate polarity-dependent charge transfer variations, according to Yoneda *et al*. [21]. Both spectra can be accurately deconvoluted into four components, which are the main sp^2 peak, two peaks shifted to higher binding energies by about 0.8 and 1.5 eV, and the C-Si peak with a binding energy about 1 eV lower than the main C-C sp^2 peak. The component at binding energy of about 1 eV higher than the sp^2 peak can be associated with the presence of a reconstructed interfacial layer between FLG and the substrate, similar to EG grown on the Si-face of SiC [32]. In contrast to the EG, this peak was observed on both the Si- and C-faces, while the EG grown on the C-face of SiC does not exhibit a components associated with the interfacial layer [33]. The peak at ~283 eV corresponding to the C-Si bonds in the SiC substrate was weak in these particular samples, indicating the FLG thickness was more than two monolayers [34].

The component shifted by 1.5 eV from the main C-C peak can be associated with C-O or C-OH bonds [35] showing that the FLG films are at least partially oxidized as a result of treatment with acids during nickel silicide removal.

B. Structural characterization of FLG films grown by SPE on SiC

The impact of varying the annealing temperature, cooling rate, substrate polarity and the thickness of the initial Ni film on the quality of the resulting FLG film was studied mainly by Raman spectroscopy. Typically, the Raman spectra of graphene films exhibit peaks in the following regions: ~1350, 1580–1590 and 2650–2750 cm^{-1}, respectively labeled D, G and 2D. The intensity of the D peak reflects the level of structural disorder in the film. The G and 2D bands confirm the presence of graphitic domains as they arise from Raman scattering events characteristic of sp^2 carbons. The G band is associated with phonon modes at the center of the Brillouin zone of graphene. The 2D band arises from a second-order Raman scattering process involving two Brillouin zone-boundary phonons [36-38].

1. Effects of annealing temperature and substrate polarity

Figure 4 shows a comparison of Raman spectra taken from FLG films formed by the silicidation of 10 nm thick Ni layers at 700, 900, 1080 ºC on the Si- (Figure 4a) and C-face (Figure 4b) of a semi-insulating 6H-SiC on-axis substrate. All spectra are normalized to the G-peak intensity. The clearly resolved G and 2D bands for the samples annealed at 900 and 1080 ºC confirm the formation of graphene on both sides of the wafer. Two effects are clear as the annealing temperature increases: the reduction of the D peak and the increase of the 2D peak relative intensities. For samples prepared at high temperatures, the lower intensity of the D peak relative to that of the G peak points to an improvement in the crystalline quality of the film. The integrated intensity ratio I_D/I_G, which is a relative measure of the film quality in terms of defect density, is quantified for each temperature and substrate polarity in Table I. The I_D/I_G ratio is reduced from 1.03 to 0.53 (C-face) and from 1.16 to 0.35 (Si-face) as the annealing temperature increases from 700 to 1080 ºC, resulting from larger domain sizes of crystalline FLG for samples annealed at the high temperature limit. The average size of sp^2 domains, L_a, in the FLG can be estimated from the I_D/I_G ratio using the equation [39]:

$$L_a\,(\mathrm{nm}) = \left(2.4\times10^{-10}\right)\lambda_{\mathrm{laser}}^{4}\left(\frac{I_{\mathrm{D}}}{I_{\mathrm{G}}}\right)^{-1} \qquad (1)$$

where λ_{laser} is the laser wavelength in nm. Also shown in Table I, the value of L_a increases from 16 to 32 nm (C-face) and from 14 to 48 nm (Si-face) for temperatures increasing from 700 to 1080 ºC.

The second effect of increasing the annealing temperature is the relative increase of the 2D peak compared to the G peak. For the sample annealed at 700 ºC the absence of a well-defined 2D peak indicates that graphene layers have not formed after the anneal. Upon increasing the temperature to 900 and 1080 ºC the 2D peak becomes clearly visible, with the sample annealed at 1080 ºC featuring the largest average crystallite size and I_{2D}/I_G intensity ratio. Comparing this ratio for the FLG films grown on different sides of the wafer, it can be concluded that the FLG films had noticeably better quality when grown on Si-face at higher temperature.

The thickness or number of monolayers, n, constituting each FLG film can be estimated from Raman spectra either by the analysis of the full width at half maximum (FWHM) of the 2D band [37, 40, 41] or the peak position of the G band [42, 43]. The FWHM values measured from the 2D peak of samples annealed at 900 and 1080 ºC (43 - 60 cm^{-1}) would suggest a FLG thickness in the region of 2 to 3 monolayers, according to the data in Hao *et al.* [41]. Alternatively, an estimate of the number of monolayers as a function of the G band position, ω_G, is given by the empirical relation [43]:

$$\omega_G\left(\mathrm{cm}^{-1}\right)=1581.6+\frac{11}{1+n^{1.6}} \quad (2)$$

Using this relation, the number of monolayers for FLG grown by annealing of 10 nm thick Ni on the Si-face at 900 (ω_G = 1583 cm^{-1}) and 1080 ºC (ω_G = 1582.5 cm^{-1}) was determined to be 3.3 and 4.6 monolayers, respectively. The same Ni film annealed on the C-face resulted in G peak positions of 1585 and 1583.5 cm^{-1} for samples annealed at 900 and 1080ºC, which correspond respectively to 1.7 and 2.7 monolayers**.** We can conclude from these measurements that the growth rate of the FLG films on the Si-face is higher than on the C-face of SiC substrate.

2. Cooling rate effect

Figure 5a shows the Raman spectra for FLG films grown on the Si-face of a 6H-SiC on-axis substrate, from a 15 nm Ni layer annealed at 1080 ºC. The figure compares samples which were cooled at a fast rate (the power was switched off and natural cooling at 28 ºC/s was allowed) and a slow rate (1 ºC/s). While almost no changes in the G and 2D peak positions, I_D/I_G ratio or $FWHM_{2D}$ values were observed, a clear increase in the I_{2D}/I_G ratio was exhibited in the spectrum taken from the sample subjected to slow cooling (I_{2D}/I_G = 1.11) compared with that with a fast cooling rate (I_{2D}/I_G = 0.69), indicating a better quality in the FLG film due to the extended cooling time. In addition to the improved I_{2D}/I_G ratio, the slow cooling also produced a shift of around 0.7 cm^{-1} in the G peak position towards lower wavenumbers, indicating that the slowly cooled sample may have developed wider FLG regions which are one monolayer thicker than the FLG obtained by fast cooling.

Further evidence of the film quality improvement is given in Figure 5b, which shows the XPS spectra comparing the fast and the slow cooling rates following annealing. The inset is a detailed view of the region between 293 and 288 eV of the main spectra, showing a shake-up satellite in the sample cooled down at a slow rate. In addition to the graphitic C-C peak at 284.5 eV, the shake-up satellite is a characteristic photoemission in graphitic carbon whereby a photoelectron with energy 284.5 eV excites a π - π^* transition, which results in a peak at ~291 eV [44]. Since the shake-up intensity is weak, it is only observed in highly graphitic crystals or regions with a high density of graphitic crystallites. Therefore, the presence of the shake-up peak in the XPS spectrum confirms the improved quality in the FLG prepared using a slow cooling rate. Finally, the weaker peak C-Si peak at ~283 eV observed in the slowly cooled sample compared with that measured in FLG

produced by fast cooling confirms the observations made by Raman spectroscopy which indicate that, on average, a slow cooling step produces a slightly thicker FLG film.

3. Impact of Ni layer thickness on layer number in FLG films

The impact of the thickness of the initial Ni layer on the FLG quality and thickness was also studied by Raman spectroscopy. Figure 6a shows typical Raman spectra taken from the FLG films formed from initial Ni layers with thicknesses of 3, 7, 10, and 20 nm. The dramatic reduction of the D peak relative intensity with increasing Ni thickness indicates a reduced density of defects in FLG films grown from thicker Ni layers. The decreasing relative intensity of the D peak with increasing Ni thickness is quantified in Table II as the integrated intensity ratio I_D/I_G. The average crystallite size was found to grow from 13 to 50 nm for Ni layers of thickness from 3 to 20 nm. It is significant that the calculated crystallite size in each sample is greater than the thickness of the initially deposited Ni. This indicates that the FLG crystallites must grow parallel to the surface.

The spectra shown in Figure 6b exhibit a prominent red-shift of the G band with increasing thickness of the initial Ni film. The estimated number of layers in FLG films was calculated using Eq. 2 and is shown in the Table II. Although it was estimated that a minimum thickness of 0.84 nm of Ni could form a graphene monolayer, in practice, our experiments demonstrate that it requires a minimum of a 3 nm thick Ni layer. Furthermore, the number of monolayers in the FLG does not appear to follow the Ni thickness in direct proportion and tends to saturate. This observation points towards a diffusion limitation of the FLG growth and will be discussed in the following section.

4. Layer stacking in FLG films

More detailed structural properties of the FLG films were revealed by further analysis of the Raman spectra. Figure 7 shows the 2D peaks from Figure 6a in more detail. It is well known that the monolayer graphene has a 2D peak at around 2700 cm^{-1}, which can be fitted with a single Lorentzian function [37]. Epitaxial FLG films grown by sublimation on the Si-face of SiC typically exhibit a 2D band shifted towards higher wave numbers compared with that of monolayer graphene, and their fitting requires a sum of Lorentzian functions, which is a signature of *AB* layer stacking in the FLG (also known as Bernal stacking) [38, 40, 41]. The multiple Lorentzian components of the 2D band in *AB* stacked films arise from the interaction between adjacent monolayers, which causes splitting in the electronic band structure of the graphene. Another typical arrangement of epitaxial FLG films is turbostratic FLG where a rotational disorder between consecutive layers exists and no *AB* stacking is observed. Unlike *AB* stacked FLG, the 2D peak for turbostratic FLG can be fitted with a single Lorentzian component essentially indistinguishable from that of a single graphene 2D

peak, because the interaction between layers is weak in non-*AB* stacking, so the electronic bands do not split into multiple branches [31, 36]. It is predicted that due to the weak interlayer interaction in turbostratic FLG, the film maintains the same electronic properties associated with single layer graphene [45]. Figure 7 also shows that SPE grown FLG is turbostratic regardless of the SiC substrate polarity, since all 2D peaks in the figure can be fitted with a single Lorentzian function, unlike EG obtained by sublimation on the Si-face of the SiC substrate, where *AB* stacking is observed. These results confirm the observations made in section 3.2.1, where the narrow XPS scans suggested that the FLG films prepared by SPE are essentially the same when grown on the Si- or the C-face of the SiC, in contrast with the polarity-dependent properties of EG.

5. Strain in FLG films

The position of the 2D bands given in Tables I and II can be used to calculate the lattice strain, ε, of the FLG films according to the equation [46]:

$$\varepsilon = -\frac{\Delta\omega_{2D}}{\omega_0 \beta_{2D} (1-\upsilon)} , \qquad (3)$$

where ω_0 is the 2D peak position for strain-free graphene, $\Delta\omega_{2D}$ is the shift of the 2D peak from ω_0, ν is the Poisson's ratio for SiC (0.183) and β_{2D} is the Grüneisen parameter for the 2D mode in graphene (2.7) [47].

No correlation between strain and the thickness of the initial Ni layer was observed. However, the 2D peak position clearly increased from 2692 to 2710 cm^{-1} with increasing growth temperature. This trend was observed in FLG films grown on both sides of the wafers and it is indicative of strain arising from the different thermal expansion rates between the graphene and the SiC substrate. The graphene was formed at the SiC/Ni_2Si interface when the SiC is expanded due to the high temperature. As the sample cools down back to room temperature, the SiC contracts. Although graphene exhibits a negative thermal expansion coefficient [48] which would cause it to expand upon cooling, it contracted at the same rate as the substrate due to it being epitaxially grown on the SiC, resulting in the FLG being compressively strained at room temperature. Therefore, FLG films grown at higher temperature exhibited accordingly higher levels of compressive strain.

The 2D peak position for FLG grown at 1080 ºC typically varied between 2705 and 2710 cm^{-1}, which corresponds to a range of compressive strain values from 0.17% to 0.24%. This value is significantly lower than the compressive strain measured in epitaxial graphene layers

grown on SiC by Si sublimation, which commonly ranges from 0.5% to 0.8% [47, 49, 50]. The lower levels of strain in SPE-grown FLG result from the significantly lower process temperature compared with epitaxial FLG obtained by sublimation. Nonetheless, the presence of residual compressive strain confirms the epitaxial nature of the FLG grown on SiC by SPE from nickel silicide supersaturated with carbon.

6. Surface morphology of FLG films

Figure 8 shows 200 nm × 200 nm AFM scans of FLG films produced from 3, 7 and 20 nm thick Ni films annealed at 1080 ºC. In Figure 8a, the surface exhibits high roughness, featuring a high concentration of hillocks which may be the origin of the intense defect band (D peak) observed in the Raman spectrum corresponding to FLG grown from a 3 nm thick Ni layer. The rms roughness for this sample was 3.47 nm. In contrast, Figures 8b and 8c present a smoother surface with only a few 1 – 2 nm high steps and R_{rms} values of 0.68 and 0.90 nm, respectively, which agree with the improved FLG quality suggested by the Raman spectra in Figure 6(a).

C. Electrical characterisation of FLG Films Grown by SPE on SiC

Resistance measurements were carried out using TLM structures fabricated on 4 μm wide FLG strips and with a separation between contact pads varying from 4 to 16 μm (inset in Figure 9). To prove that there is no contribution from current through the substrate, structures without graphene strips between nickel silicide contacts were also fabricated side-by-side with the TLM structures. The resistance measured between these contact pads was on the order of 10^7 Ω, which confirmed that the conductivity through the substrate can be neglected. The plot in Figure 9 presents the FLG film resistance (R_T) as a function of the distance for the FLG film grown from an initially 7 nm thick Ni layer on the C-face of a semi-insulating 6H-SiC substrate at 1080 °C. The R_T value demonstrated a linear dependence on the separation distance between nickel silicide contacts (d). A linear fit of the data in Figure 9 can be expressed as [51]:

$$R_T = \rho_{sh}\left(\frac{d}{W}\right) + 2\frac{\rho_C}{WL_T} \qquad (4)$$

where ρ_{sh} is the FLG sheet resistance, W is the width of the FLG strip, ρ_c is the contact resistivity, and L_T is the transfer length defined as $L_T = \sqrt{\frac{\rho_C}{\rho_{sh}}}$. The values of ρ_c, ρ_{sh} and L_T extracted from the plot using this expression were 3.5×10^{-3} Ω·cm^2, 10.5×10^3 Ω □$^{-1}$ and 5.8 μm, respectively.

The van der Pauw structures for Hall measurement were fabricated on FLG films formed by annealing of a 7 nm thick Ni layer on the C-face of a 6H-SiC on-axis semi-insulating substrate at 1080 ºC. The patterned squares of FLG films with Ni_2Si self-aligned contacts and Ti/Ag contact enforcement had side lengths of 30 μm and 60 μm (shown in the inset of Figure 10). Figure 10 shows the resulting mobility values measured at magnetic fields from 0.1 to 0.3 T. Mobilities of 50 and 30 cm^{2}V^{-1}s^{-1} were obtained for the 30 μm and 60 μm squares, respectively. The sheet resistance values measured in the 30 μm and 60 μm squares were 9.8×10^3 and 10.5×10^3 Ω □$^{-1}$, respectively, close to the sheet resistance measured by TLM. The charge carriers in the fabricated FLG films were determined to be holes with the sheet carrier density ranging from 1 to 2×10^{13} cm^{-2}.

D. Discussion

It was clearly shown by XPS and Raman spectroscopy that the FLG films were grown at the interface between the SiC substrate and the reaction zone. On the other hand, the FLG films formed in the same reaction have also been found on the surface of the unreacted nickel and have even been transferred onto foreign insulating substrates [19]. Furthermore, it is well known that the interaction of nickel with silicon carbide is a diffusion-controlled process [52] and that nickel is the most mobile species in the intermetallic compounds forming the reaction zone [53, 54]. Therefore, during the reaction the interface between the reaction zone and the SiC substrate keeps moving into the silicon carbide, away from the initial Ni/SiC interface (Kirkendall plane), as was clearly shown in marker experiments [17]. Obviously, the formation of a FLG film in a moving interface is not possible. This contradiction can be easily explained by a simple model based on two experimental observations: (1) the quality of FLG films depended on growth temperature as well as on cooling rate, and (2) the number of layers in the FLG films did not follow the Ni thickness in direct proportion and tended to saturate. It should be noted also that even Ni films up to 10 times as thick as those used in this work also produced FLG films with estimated thicknesses of just 2 - 4 layers [23]. These facts lead to the conclusion that only a fraction of the released carbon atoms participate in formation of FLG films, following the process shown schematically in Figure 11. Indeed, assuming that an initial Ni/SiC system (shown in Figure 11a) has a nickel layer sufficiently thick to create a reasonable number of

layers in a FLG film, a solid phase chemical reaction starts when this structure is subjected to heating at temperatures above 600 °C, and a reaction zone is created (Figure 11b). This reaction zone consists of Ni_2Si saturated with carbon and immovable carbon precipitates which form because carbon does not create nickel carbide and has low solubility in Ni_2Si. At this stage, two diffusion flows in opposite directions exist: (1) nickel atoms diffuse through the reaction zone towards the SiC interface to support the reaction and (2) carbon atoms diffuse from the reaction zone into the nickel layer. The solubility of carbon in nickel is even lower than in nickel silicide (respectively about 0.2% versus 0.8-1% at 450 °C, see ref. [15, 25]), therefore, the nickel layer is easily saturated with carbon. While the nickel layer becomes thinner due to its consumption by the solid phase reaction, the concentration of carbon atoms at the surface of the nickel layer exceeds a solubility limit resulting in the formation of carbon precipitates or a FLG film. Obviously, the thickness of this FLG film has to depend on the thickness of the initial nickel layer, the process temperature and duration. The growth of this FLG film may be interrupted at the stage shown in Figure 11b or it may stop on its own when all the nickel is consumed (Figure 11c). Finally, the FLG film in the Ni_2Si/SiC interface is formed during cooling (Figure 11d). The solubility of carbon in Ni_2Si reduces with decreasing temperature and nickel silicide becomes supersaturated with carbon, which has to be released either in the form of precipitates or a FLG film at the SiC interface. As confirmed by the experiment comparing fast and slow cooling rates after annealing, the thickness of this FLG film is determined by the process temperature and cooling rate rather than the nickel and reaction zone thicknesses. This qualitative model reasonably explains the detection of FLG films either in the Ni_2Si/SiC interface or on the surface of unreacted nickel. Further in depth quantitative analysis of reaction kinetics is beyond the scope of this paper.

Another topic which requires discussion is the conductivity type of the FLG films produced by SPE. The conductivity type of EG is mainly defined by two factors: the charge transfer from the substrate [55] and from metals used for fabrication of ohmic contacts.[56] Both silicon carbide and titanium (which are commonly used to form ohmic contacts to graphene) have work functions lower than that of graphene (4.6 eV [57]). This results in the transfer of electrons from the contacts and substrate into graphene until the Fermi levels are aligned. These electrons define the n-type of graphene conductivity. In contrast, the FLG films fabricated in this work revealed a p-type conductivity. The most probable reason for this change of conductivity type is the modification of FLG films by chemical treatment. Indeed, to remove the nickel silicide and to form self-aligned contacts, the samples were etched in mixture of strong acids followed by rinsing in photoresist solvents and water. Chemical modification of the FLG films was confirmed by XPS clearly showing the presence of carbon-oxygen bonds. Oxygen acts as an electron-withdrawing adsorbate

and leads to the hole conductivity in graphene, as it has been reported elsewhere [58]. Furthermore, the work function of Ni_2Si, which composes the self-aligned contacts in the FLG films, is equal to 4.94 eV [59]. This value is higher than that of graphene and the Fermi level in the FLG film has to be shifted below the Dirac point to match with the contacts, which also results in p-type conductivity.

Finally, it has to be admitted that the mobility measured in fabricated FLG films does not compare favourably with those reported for EG. The nature of solid phase epitaxy and the unavoidable impact of removing nickel silicide in strong acids makes it unlikely to produce FLG films with a quality comparable to EG. Nevertheless, the p-type conductivity clearly indicates that the fabricated films are few layer graphene rather than nickel silicide residuals or sedimentary layers of graphite precipitates. These FLG films grown by SPE can find their own niche of applications. Indeed, owing to the fabrication by local SPE, these FLG films can be easily patterned, grown on insulating, chemically inert substrates and have self-aligned ohmic contacts with low resistivity. It is possible to integrate these FLG films in silicon carbide electronics due to their device processing compatibility. The presence of polar oxygen-containing functional groups at the surface of these FLG films allows their further chemical modification or functionalization and makes them attractive for various applications in sensitive electrochemical systems, bio- and chemical sensors.

SUMMARY

Patterned few-layer graphene (FLG) films were grown by local solid phase epitaxy (SPE) on semi-insulating 6H-SiC substrates from nickel silicide supersaturated with carbon. FLG films were grown at the interface between nickel silicide and silicon carbide both on silicon- and carbon-terminated faces of the substrates. The growth process was followed by selective wet etching of nickel silicide to form self-aligned ohmic contacts. It was shown by Raman spectroscopy and XPS that the process temperature (ranging from 700 to 1080 °C) and cooling rate significantly affected the final quality of FLG films. It was found that the number of layers in the FLG films did not follow the Ni thickness in direct proportion and tended to saturate, although the FLG films grown from thicker Ni layers exhibited lower roughness and larger sp^2 domain size. The FLG films exhibited compressive strain which increased with the growth temperature but was significantly lower than that in graphene grown on SiC by sublimation. Comparison of these experimental results led to the conclusion that the FLG films were grown during the cooling stage of the process rather than during the dwelling time at high temperature. A simple qualitative model of diffusion-driven solid phase chemical reaction was proposed to explain the formation of FLG films at the surface of

unreacted nickel (reported elsewhere) and at the interface between the reaction zone and silicon carbide substrate.

The resulting FLG films were free of residual nickel silicide but had singly bonded oxygen (C-OH or C-O-C groups) on the surface, as detected by XPS. The TLM and van der Pauw structures with self-aligned nickel silicide contacts were used for the electrical characterization of the FLG, which was carried out on-wafer at room temperature. The self-aligned nickel silicide contacts revealed reasonably low contact resistivity of 3.5×10^{-3} $\Omega\cdot cm^2$. The FLG films exhibited p-type conductivity with carrier Hall mobilities of 50 $cm^2V^{-1}s^{-1}$ and sheet concentrations of 10^{13} cm^{-2}. The low Hall mobility was most likely caused by the relatively small size of sp^2 domains resulting from the nature of solid phase epitaxy and the partial oxidation of the FLG films, as a result of the removal of nickel silicide in strong acids. Nevertheless, this is the first direct measurement of charge transport properties in FLG films fabricated by SPE on SiC from nickel silicide and it irrefutably confirms that these films are few layer graphene rather than nickel silicide residuals or sedimentary layers of carbon precipitates. These FLG films can find their own niche of applications due to easy integration of SPE in standard device processing, and thus, further development of this graphene growth technique is of great interest.

ACKNOWLEDGMENT

This work was supported by the Leverhulme Trust (grant F/00 125/AN).

TABLES

TABLE I. Integrated intensity ratios I_D/I_G and I_{2D}/I_G, average crystallite size, and full width half maximum calculated from Raman spectra on FLG films grown from 10 nm thick Ni layers at annealing temperatures of 700, 900, and 1080 ℃.

	Temperature (°C)	**ω_G (cm^{-1})**	***n***	**I_D/I_G**	**ω_{2D} (cm^{-1})**	**I_{2D}/I_G**	**L_a (nm)**	**$FWHM_{2D}$ (cm^{-1})**
	700	1597.0		1.16	2695	0.10	14	100
Si-face	900	1583.0	3.3	0.65	2966	0.36	26	62
	1080	1582.5	4.6	0.35	2705	0.69	48	43
	700	1595.0		1.03	2692	0.09	16	96
C-face	900	1585.0	1.7	0.71	2703	0.39	24	60
	1080	1583.5	2.7	0.53	2710	0.48	32	51

TABLE II. Integrated intensity ratios I_D/I_G and I_{2D}/I_G, average crystallite size, and full width half maximum calculated from Raman spectra on FLG films grown on the C-face of the SiC substrate from Ni layers with thicknesses varying from 3 to 20 nm.

Ni thickness (nm)	**ω_G (cm^{-1})**	***n***	**I_D/I_G**	**L_a (nm)**	**ω_{2D} (cm^{-1})**	**I_{2D}/I_G**	**$FWHM_{2D}$ (cm^{-1})**
3	1587.0	1	1.26	13	2704	0.91	56
7	1585.5	1.5	0.92	18	2708	0.86	46
10	1583.5	2.7	0.53	32	2710	0.48	51
15	1585.0	1.7	0.29	58	2708	0.69	36
20	1583.0	3.3	0.33	50	2708	1.11	47

FIGURES

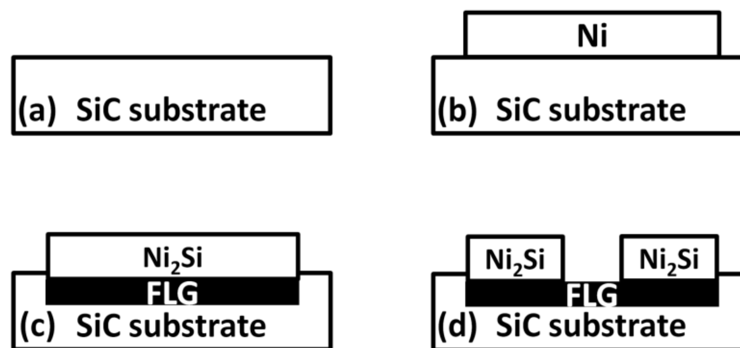

Figure 1. Schematic representation (not in scale) of the local solid phase epitaxy of few-layer graphene films on silicon carbide: (a) initial SiC substrate; (b) Ni deposition, which can be patterned; (c) annealing to form Ni_2Si and the FLG film; and (d) selective wet etching of Ni_2Si to produce FLG structures with self-aligned contacts.

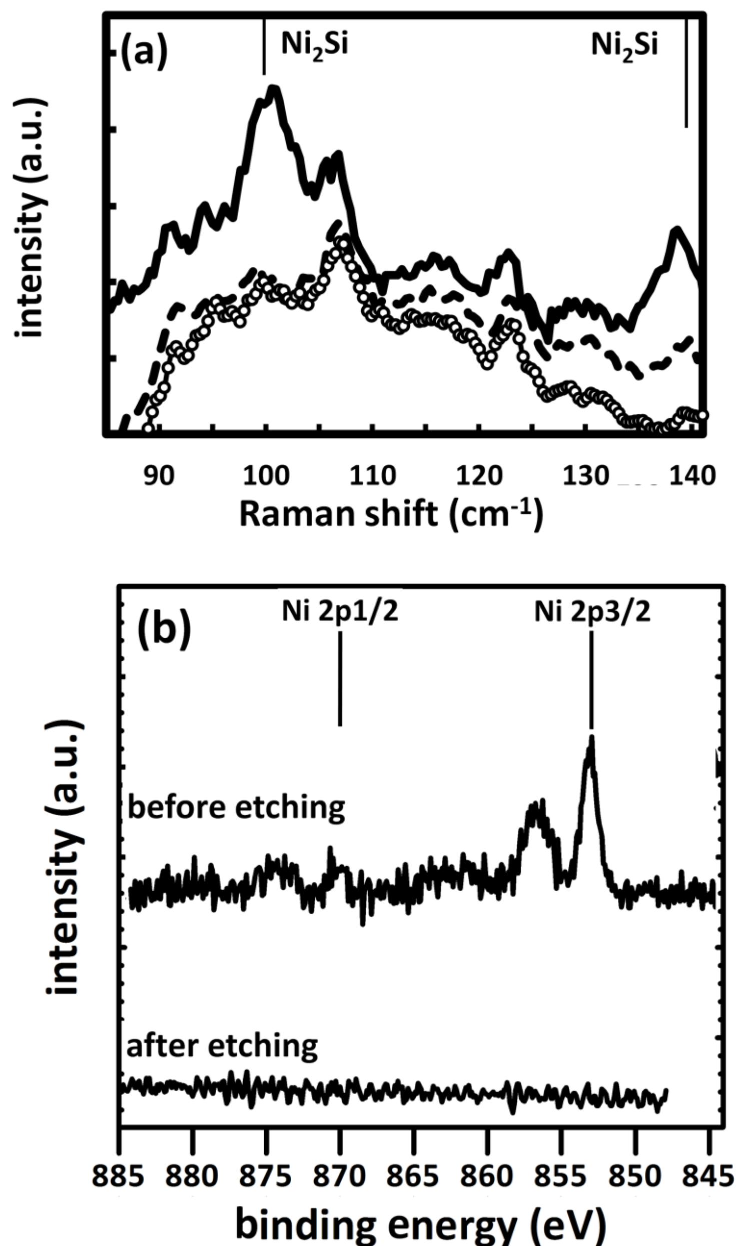

Figure 2. (a) Raman spectrum showing the characteristic peaks of Ni_2Si at 100 cm^{-1} and 140 cm^{-1} compared with the spectra of the 20 nm thick Ni film as-deposited before annealing (dashed line) and the FLG film following the wet etch removal of the Ni_2Si (line with circles). (b) XPS Ni 2*p* scans measured on the FLG before and after Ni_2Si wet etching, confirming the complete removal of Ni_2Si.

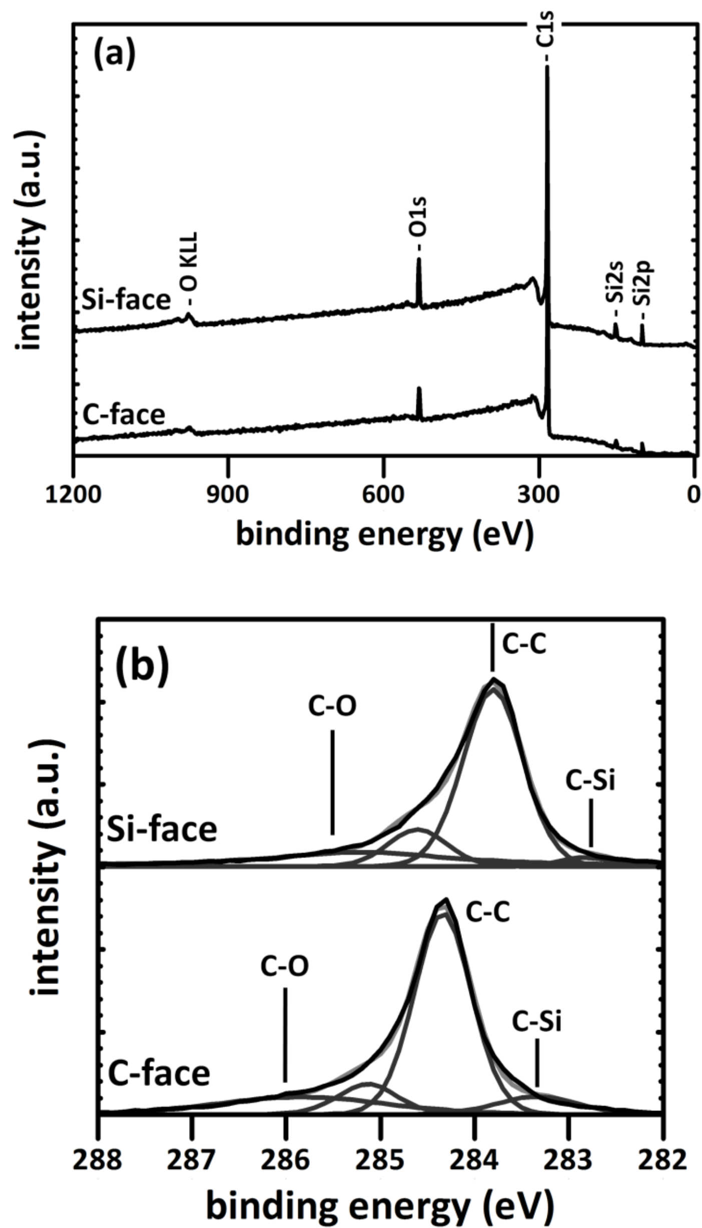

Figure 3. XPS spectra of a FLG film grown on the Si- and C-face of a 6H-SiC on-axis substrate from an initial Ni layer thickness of 7 nm and annealed at 1080 ºC. (a) Survey scan showing the main species on the samples; (b) narrow C1*s* scan after background subtraction showing peaks assigned to the existence of C-C sp^2.

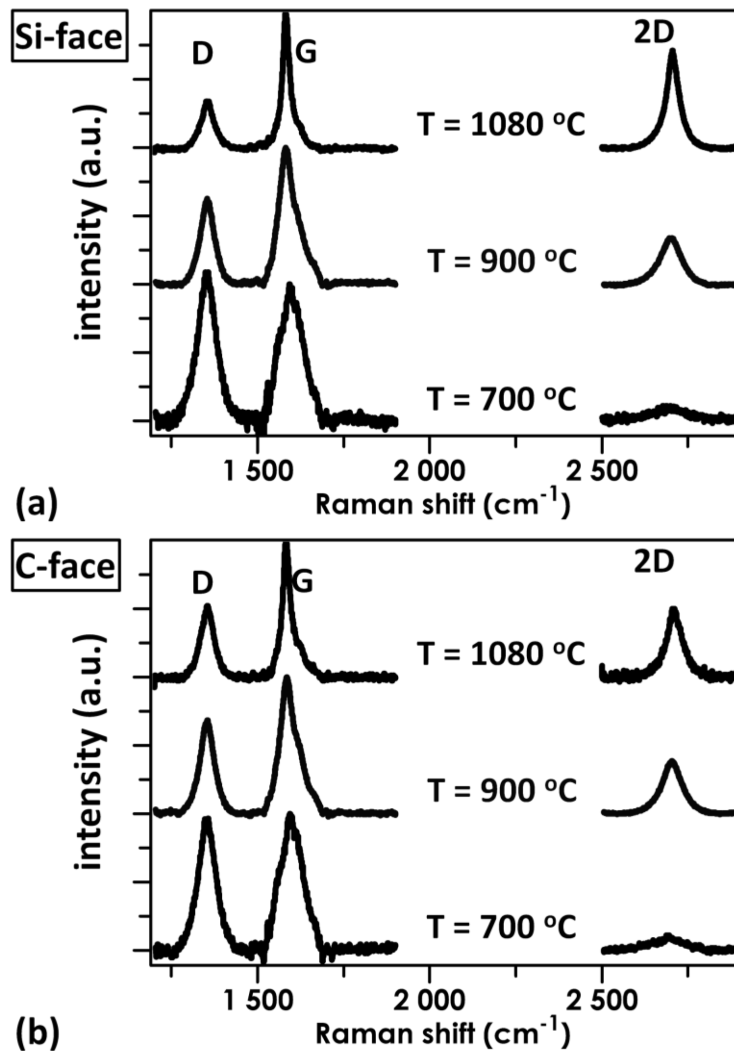

Figure 4. Raman spectra taken from the FLG film grown on the Si-face of a semi-insulating 6H-SiC on-axis substrate. 10 nm thick Ni layers were annealed at 700, 900, and 1080 ºC in vacuum. Spectra are normalized to the G-peak intensity. The FLG films were grown on: (a) the Si-face and (b) the C-face of the 6H-SiC substrate.

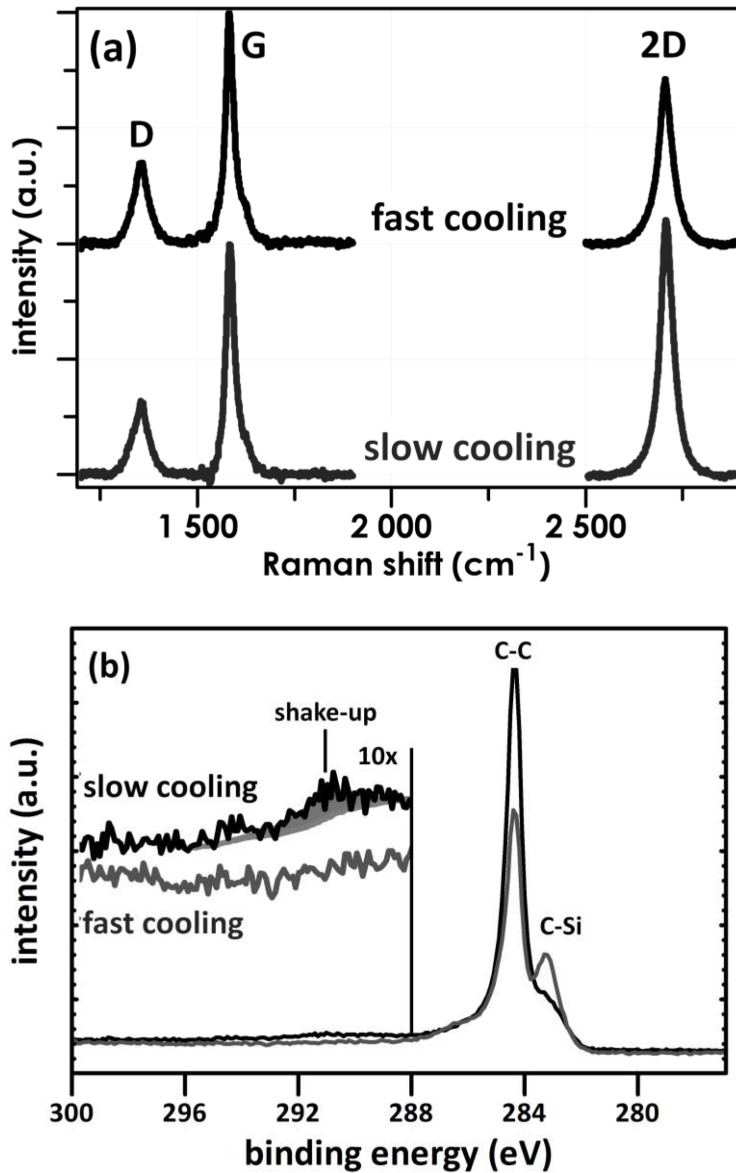

Figure 5. (a) Raman spectra and (b) XPS spectra comparing FLG films grown on the Si-face of a 6H-SiC on-axis substrate from an initial Ni layer thickness of 15 nm, annealed at 1080 ºC and cooled down at a fast rate (28 ºC/s, gray line) and a slow rate (1 ºC/s, black line). The inset in (b) is a 10× magnification of the region between 293 and 288 eV of the main spectra, showing the shake-up satellite in the sample cooled down at a slow rate. The filled-in component is a Lorentzian fit of the shake-up peak.

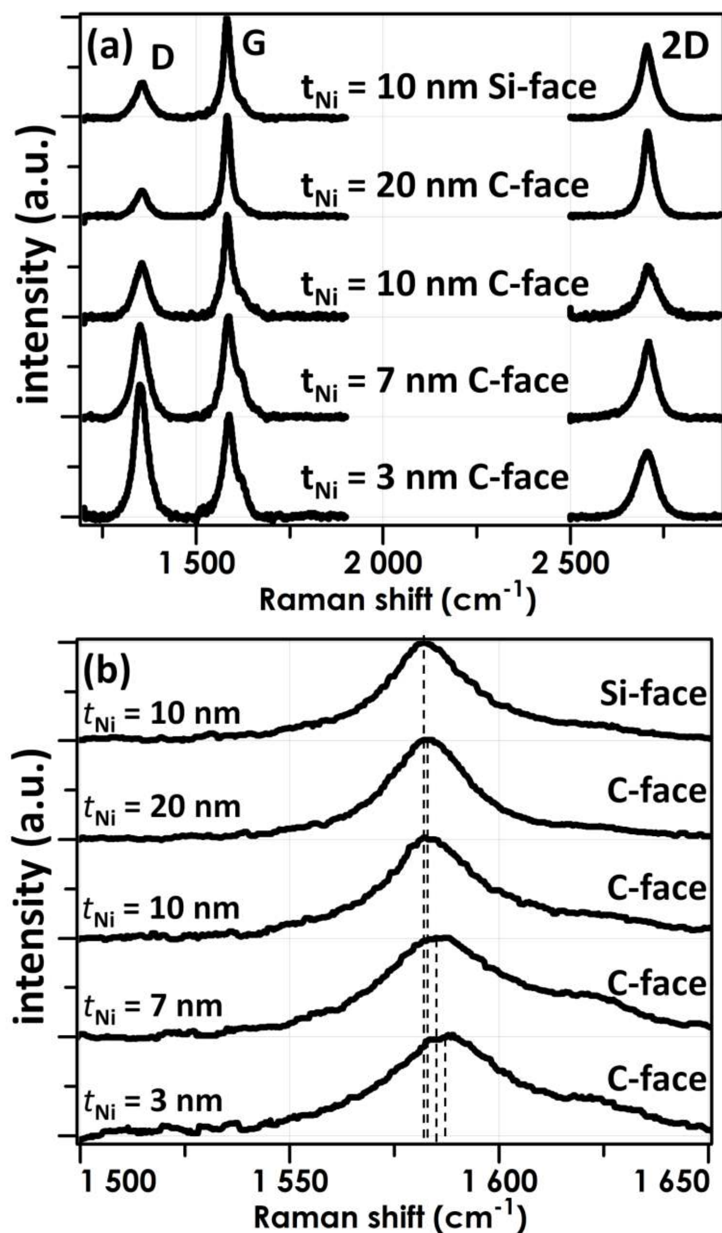

Figure 6. (a) Raman spectra from the FLG film grown on the Si- and C-face of a 6H-SiC on-axis substrate. The SiC substrate signal was subtracted. (b) Detail of the spectral region from 1500 cm^{-1} to 1650 cm^{-1} highlighting the red-shift of the G peak with increasing thickness of the initial Ni layer.

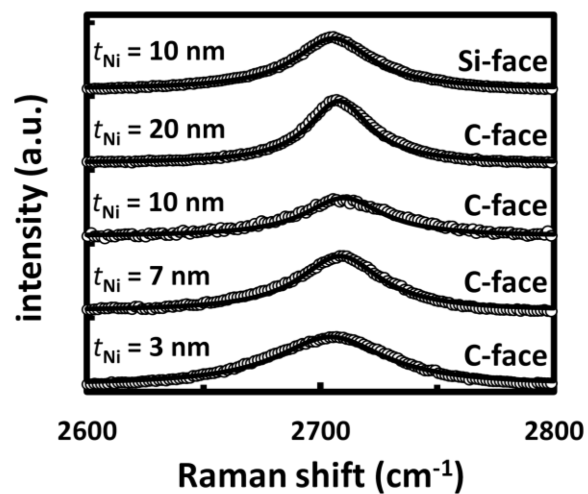

Figure 7. Raman spectra from the FLG film grown on the Si- and C-face of a 6H-SiC on-axis substrate, showing the fitting of the 2D band to a single Lorentzian function (gray line).

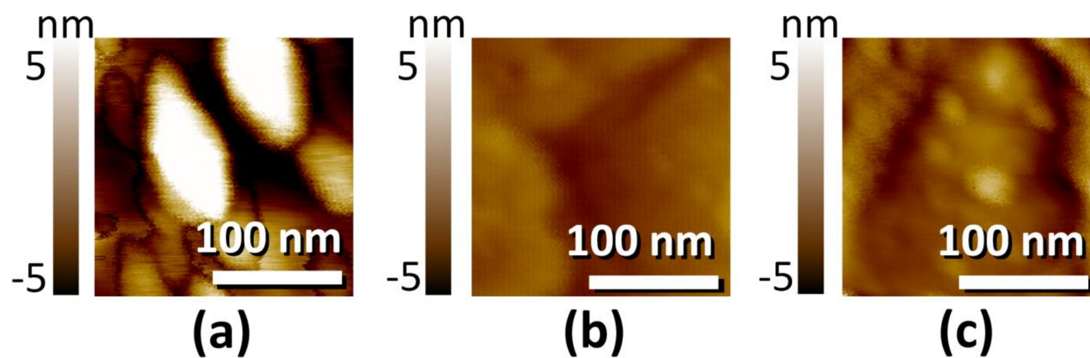

Figure 8. AFM images of FLG films formed on the C-face of a 6H-SiC on-axis substrate from initial Ni film thicknesses of (a) 3 nm, (b) 7 nm and (c) 20 nm, annealed at 1080 ºC.

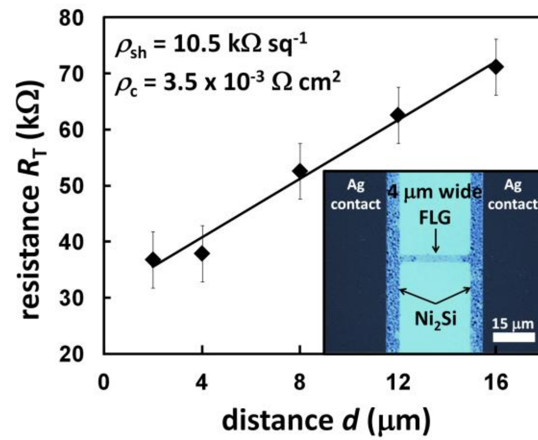

Figure 9. Resistance of the FLG film measured on TLM structures. The FLG film was formed on the C-face of a 6H-SiC on-axis substrate from a 7 nm thick Ni layer, annealed at 1080 ºC. Inset: optical micrograph of a section of the TLM structure showing the 4 μm wide FLG stripes between contacts.

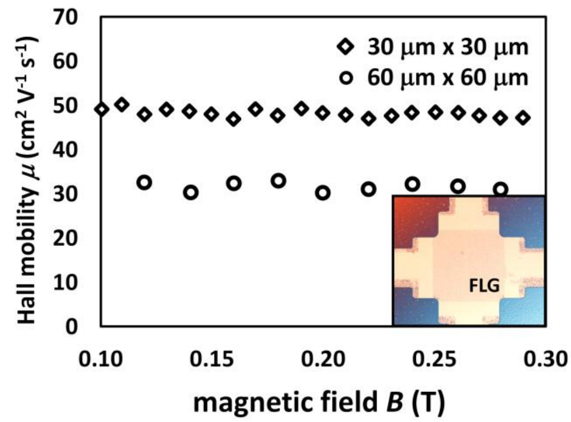

Figure 10. Hall mobility measured on patterned square-shaped FLG areas of 30 μm × 30 μm and 60 μm × 60 μm in the magnetic field range between 0.1 to 0.3 T. The FLG films were formed on the C-face of a 6H-SiC on-axis substrate from a 7 nm thick Ni layer, annealed at 1080 ºC. Inset: optical micrograph of the Hall test structure showing the square FLG pattern at the center and Ni_2Si/Ti/Ag contacts at each of its corners.

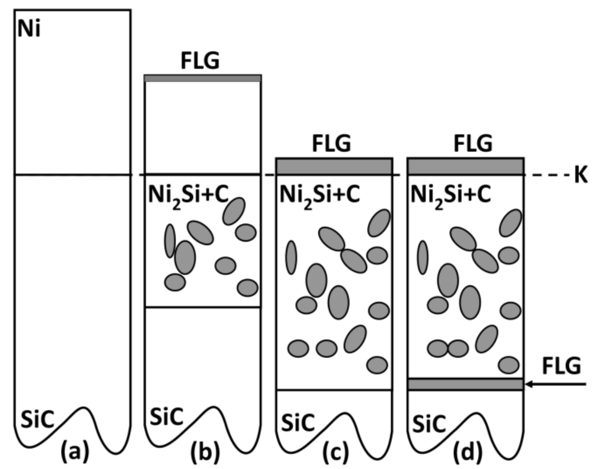

Figure 11. Schematic image of structural evolution in the Ni/SiC system during annealing. K denotes the Kirkendall plane.

REFERENCES

1. A. K. Geim, Science **324** (5934), 1530-1534 (2009).
2. K. S. Novoselov, A. K. Geim, S. V. Morozov, D. Jiang, Y. Zhang, S. V. Dubonos, I. V. Grigorieva and A. A. Firsov, Science **306** (5696), 666-669 (2004).
3. F. Schedin, A. K. Geim, S. V. Morozov, E. W. Hill, P. Blake, M. I. Katsnelson and K. S. Novoselov, Nat Mater **6** (9), 652-655 (2007).
4. X. Wang, L. Zhi and K. Mullen, Nano Letters **8** (1), 323-327 (2007).
5. Z.-S. Wu, W. Ren, L. Gao, B. Liu, C. Jiang and H.-M. Cheng, Carbon **47** (2), 493-499 (2009).
6. A. Reina, X. Jia, J. Ho, D. Nezich, H. Son, V. Bulovic, M. S. Dresselhaus and J. Kong, Nano Letters **9** (1), 30-35 (2008).
7. C. Berger, Z. Song, T. Li, X. Li, A. Y. Ogbazghi, R. Feng, Z. Dai, A. N. Marchenkov, E. H. Conrad, P. N. First and W. A. de Heer, The Journal of Physical Chemistry B **108** (52), 19912-19916 (2004).
8. K. V. Emtsev, A. Bostwick, K. Horn, J. Jobst, G. L. Kellogg, L. Ley, J. L. McChesney, T. Ohta, S. A. Reshanov, J. Rohrl, E. Rotenberg, A. K. Schmid, D. Waldmann, H. B. Weber and T. Seyller, Nat Mater **8** (3), 203-207 (2009).
9. J. L. Tedesco, B. L. VanMil, R. L. Myers-Ward, J. C. Culbertson, G. G. Jernigan, P. M. Campbell, J. M. McCrate, S. A. Kitt, J. C.R. Eddy and D. K. Gaskill, Mater. Sci. Forum **615-617**, 211 (2009).
10. I. P. Nikitina, K. V. Vassilevski, N. G. Wright, A. B. Horsfall, A. G. O'Neill and C. M. Johnson, Journal of Applied Physics **97** (8), 083709-083707 (2005).
11. I. Nikitina, K. Vassilevski, A. Horsfall, N. Wright, A. G. O'Neill, S. K. Ray, K. Zekentes and C. M. Johnson, Semiconductor Science and Technology **24** (5), 055006 (2009).
12. I. Nikitina, K. Vassilevski, A. Horsfall, N. Wright, A. G. O'Neill, S. K. Ray and C. M. Johnson, in *Materials Science Forum* (2009), Vol. 615-617, pp. 577-580.
13. K. Vassilevski, K. P. Hilton, N. Wright, M. Uren, A. Munday, I. Nikitina, A. Hydes, A. Horsfall and C. M. Johnson, in *Materials Science Forum*, edited by A. Suzuki, H. Okumura, T. Kimoto, T. Fuyuki, K. Fukuda and S. Nishizawa (2009), Vol. 600-603, pp. 1063-1066.
14. R. C. J. Schiepers, F. J. J. v. Loo and G. d. With, J. Am. Ceram. Soc. **71**, C284 (1988).
15. J. J. Lander, H. E. Kern and A. L. Beach, Journal of Applied Physics **23** (12), 1305-1309 (1952).
16. L. Calcagno, E. Zanetti, F. L. Via, F. Roccaforte, V. Raineri, S. Libertino, F. Giannazzo, M. Mauceri and P. Musumeci, Materials Science Forum **433-436,**, 721 (2003).
17. I. P. Nikitina, K. V. Vassilevski, A. B. Horsfall, N. G. Wright, A. G. O’Neill, C. M. Johnson, T. Yamamoto and R. K. Malhan, Semiconductor Science and Technology **21** (7), 898-905 (2006).
18. S. Y. Han, K. H. Kim, J. K. Kim, H. W. Jang, K. H. Lee, N. K. Kim, E. D. Kim and J. L. Lee, Applied Physics Letters **79**, 1816 (2001).
19. Z.-Y. Juang, C.-Y. Wu, C.-W. Lo, W.-Y. Chen, C.-F. Huang, J.-C. Hwang, F.-R. Chen, K.-C. Leou and C.-H. Tsai, Carbon **47** (8), 2026-2031 (2009).
20. A. A. Woodworth and C. D. Stinespring, Carbon **48** (7), 1999-2003 (2010).
21. T. Yoneda, M. Shibuya, K. Mitsuhara, A. Visikovskiy, Y. Hoshino and Y. Kido, Surface Science **604** (17–18), 1509-1515 (2010).
22. C. Y. Kang, L. L. Fan, S. Chen, Z. L. Liu, P. S. Xu and C. W. Zou, Applied Physics Letters **100** (25), 251604-251604-251605 (2012).
23. P. Macháč, T. Fidler, S. Cichoň and L. Mišková, Thin Solid Films **520** (16), 5215-5218 (2012).
24. K. Vassilevski, I. P. Nikitina, A. B. Horsfall, N. G. Wright and C. M. Johnson, Materials Science Forum **645 - 648**, 589 - 592 (2010).

25. A. Hähnel, V. Ischenko and J. Woltersdorf, Materials Chemistry and Physics **110** (2-3), 303-310 (2008).
26. E. Escobedo-Cousin, K. Vassilevski, I. P. Nikitina, N. G. Wright, A. G. O'Neill, A. B. Horsfall and J. P. Goss, Materials Science Forum **717-720**, 629-632 (2012).
27. I. o. www.tankeblue.com.
28. I. o. www.novasic.com.
29. M. Qin, M. C. Poon and C. Y. Yuen, Sensors and Actuators A: Physical **87**, 90-95 (2000).
30. E. Kurimoto, H. Harima, T. Toda, M. Sawada, M. Iwami and S. Nakashima, Journal of Applied Physics **91** (12), 10215-10217 (2002).
31. Y. Cao, L. Nyborg and U. Jelvestam, Surface and Interface Analysis **41** (6), 471-483 (2009).
32. K. V. Emtsev, F. Speck, T. Seyller, L. Ley and J. D. Riley, Physical Review B **77** (15), 155303 (2008).
33. L. B. Biedermann, M. L. Bolen, M. A. Capano, D. Zemlyanov and R. G. Reifenberger, Physical Review B **79** (12), 125411 (2009).
34. J. Penuelas, A. Ouerghi, D. Lucot, C. David, J. Gierak, H. Estrade-Szwarckopf and C. Andreazza-Vignolle, Physical Review B **79** (3), 033408 (2009).
35. A. Ganguly, S. Sharma, P. Papakonstantinou and J. Hamilton, The Journal of Physical Chemistry C **115** (34), 17009-17019 (2011).
36. F. Tuinstra and J. L. Koenig, Journal of Chemical Physics **53** (3), 1126-1130 (1970).
37. A. C. Ferrari, J. C. Meyer, V. Scardaci, C. Casiraghi, M. Lazzeri, F. Mauri, S. Piscanec, D. Jiang, K. S. Novoselov, S. Roth and A. K. Geim, Physical Review Letters **97** (18), 187401 (2006).
38. M. S. Dresselhaus, A. Jorio, M. Hofmann, G. Dresselhaus and R. Saito, Nano Letters **10** (3), 751-758 (2010).
39. L. G. Cançado, K. Takai, T. Enoki, M. Endo, Y. A. Kim, H. Mizusaki, A. Jorio, L. N. Coelho, R. Magalhaes-Paniago and M. A. Pimenta, Applied Physics Letters **88** (16), 163106-163103 (2006).
40. D. Graf, F. Molitor, K. Ensslin, C. Stampfer, A. Jungen, C. Hierold and L. Wirtz, Nano Letters **7** (2), 238-242 (2007).
41. Y. Hao, Y. Wang, L. Wang, Z. Ni, Z. Wang, R. Wang, C. K. Koo, Z. Shen and J. T. L. Thong, Small **6** (2), 195-200 (2010).
42. A. Gupta, G. Chen, P. Joshi, S. Tadigadapa and Eklund, Nano Letters **6** (12), 2667-2673 (2006).
43. H. Wang, Y. Wang, X. Cao, M. Feng and G. Lan, Journal of Raman Spectroscopy **40** (12), 1791-1796 (2009).
44. P. Machac, T. Fidler, S. Cichon and L. Miskova, Thin Solid Films **520** (16), 5215-5218 (2012).
45. J. Hass, F. Varchon, J. E. Millán-Otoya, M. Sprinkle, N. Sharma, W. A. de Heer, C. Berger, P. N. First, L. Magaud and E. H. Conrad, Physical Review Letters **100** (12), 125504 (2008).
46. Z. H. Ni, T. Yu, Y. H. Lu, Y. Y. Wang, Y. P. Feng and Z. X. Shen, ACS Nano **2** (11), 2301-2305 (2008).
47. L. O. Nyakiti, R. L. Myers-Ward, V. D. Wheeler, E. A. Imhoff, F. J. Bezares, H. Chun, J. D. Caldwell, A. L. Friedman, B. R. Matis, J. W. Baldwin, P. M. Campbell, J. C. Culbertson, C. R. Eddy, G. G. Jernigan and D. K. Gaskill, Nano Letters **12** (4), 1749-1756 (2012).
48. D. Yoon, Y.-W. Son and H. Cheong, Nano Letters **11** (8), 3227-3231 (2011).
49. N. Ferralis, R. Maboudian and C. Carraro, Physical Review Letters **101** (15), 156801 (2008).
50. J. A. Robinson, M. Wetherington, J. L. Tedesco, P. M. Campbell, X. Weng, J. Stitt, M. A. Fanton, E. Frantz, D. Snyder, B. L. VanMil, G. G. Jernigan, R. L. Myers-Ward, C. R. Eddy and D. K. Gaskill, Nano Letters **9** (8), 2873-2876 (2009).
51. D. K. Schroder, *Semiconductor material and decive characterization*, 2nd ed. (1998).
52. F. Goesman and R. Schmid-Fetzer, Mat. Sc. and Eng B **46**, 357-362 (1997).

53. M. Levit, I. Grimberg and B.-Z. Weiss, J. Appl. Phys. **80**, 167-173 (1996).
54. A. A. Kodentsov, M. R. Rijnders and F. J. J. Van Loo, Acta Materialia **46** 6521-6528 (1998).
55. S. Kopylov, A. Tzalenchuk, S. Kubatkin and V. I. Fal'ko, Applied Physics Letters **97** (11), 112109-112103 (2010).
56. J. S. Moon, M. Antcliffe, H. C. Seo, D. Curtis, S. Lin, A. Schmitz, I. Milosavljevic, A. A. Kiselev, R. S. Ross, D. K. Gaskill, P. M. Campbell, R. C. Fitch, K. M. Lee and P. Asbeck, Applied Physics Letters **100** (20), 203512-203513 (2012).
57. N. Chuhei Oshima and Ayato, Journal of Physics: Condensed Matter **9** (1), 1 (1997).
58. Y. Yang, K. Brenner and R. Murali, Carbon **50** (5), 1727-1733 (2012).
59. Y.-J. Chang and J. L. Erskine, Physical Review B **28** (10), 5766-5773 (1983).